Supporting Information for

Molecular Magnetic Resonance Imaging Using a Redox Active Iron Complex

Huan Wang, [‡1] Veronica Clavijo Jordan, [‡1,2] Ian A. Ramsay, [‡1] Mozhdeh Sojoodi,[3] Bryan C. Fuchs,[3] Kenneth K. Tanabe,[3] Peter Caravan,[1,2] and Eric M. Gale*[1]

[1]Athinoula A. Martinos Center for Biomedical Imaging, Department of Radiology, Massachusetts General Hospital/ Harvard Medical School, 149 Thirteenth Street, Charlestown, MA 02129. [2]Institute for Innovation in Imaging, Department of Radiology, Massachusetts General Hospital, 55 Fruit Street, Boston, MA 02114. [3]Division of Surgical Oncology, Massachusetts General Hospital/ Harvard Medical School, WRN401, 55 Fruit Street, Boston, MA 02114.

‡Authors contributed equally

*Correspondence: egale@nmr.mgh.harvard.edu

General. All chemicals and solvents were purchased commercially and used without further purification.

NMR. NMR spectra were recorded on a 500 MHz Varian spectrometer. Chemical shifts are reported in δ (ppm). For ^{1}H and ^{13}C NMR spectra, the residual solvent peaks were used as internal reference except for ^{13}C NMR recorded in D_2O where *tert*-BuOH was used as the internal reference.[1] Relaxivity measurements were performed on a Bruker mq60 Minispec, 1.41 T, and on a 11.7 T Varian NMR spectrometer, at 37 °C. Longitudinal (T_1) relaxation times were measured via an inversion recovery experiment using 10 inversion times of duration ranging between 0.05 x T_1 and 5 x T_1; transverse (T_2) relaxation times were measured using a Carr-Purcell-Meiboom-Gill spin-echo experiment. Relaxivity (r_i, i=1,2) was determined from the slope of a plot of $1/T_i$ (i=1,2) vs. [Fe] for at least 4 concentrations. The transverse (T_2) relaxation times of $H_2{}^{17}O$ were acquired at 11.7 T using a CPMG pulse sequence at temperatures ranging from 283 to 348 K. Samples were prepared in neat H_2O adjusted and enriched with a small amount of $H_2{}^{17}O$. The ^{17}O hyperfine coupling constant for the Fe^{2+}-OH_2 interaction was estimated from the concentration dependence on the Fe induced chemical shift ($\Delta\omega_m$) of the bulk $H_2{}^{17}O$ resonance at 40 °C, according to eqs S4 and S5, below. Reduced relaxation rates ($1/T_{2r}$) were calculated by dividing the Fe^{2+}-PyC3A or Fe^{3+}-PyC3A imparted increase in $1/T_2$ relative to neat H_2O at pH 3 by the mole fraction of the Fe complex, eq S1. This data was plotted against reciprocal temperature (1000/T (K^{-1})) and fit to the Swift-Connick equations describing 2-site exchange,[2] as described below, and applied previously.[3-7]

Influence of paramagnetic Fe on ^{17}O NMR data. The presence of a paramagnetic complex will influence both the transverse relaxation and chemical shift of the bulk $H_2{}^{17}O$ NMR signal according to eqs S11-2 below,

$$\frac{1}{T_{2r}} = \frac{1}{P_m}\left(\frac{1}{T_2} - \frac{1}{T_2^0}\right) = k_{ex}\left[\frac{T_{2m}^{-2} + \left(\frac{k_{ex}}{T_{2m}}\right) + \Delta\omega_m^2}{\left(T_{2m}^{-1} + k_{ex}\right)^2 + \Delta\omega_m^2}\right] + \frac{1}{T_{2os}} \quad \text{(Eq S1)}$$

$$\Delta\omega_r = \frac{1}{P_m}(\Delta\omega_m - \Delta\omega_o) = \frac{\Delta\omega_m}{\left(1 + k_{ex}^{-1}T_{2m}^{-1}\right) + \Delta\omega_m^2/k_{ex}^2} + \Delta\omega_{os} \quad \text{(Eq S2)}$$

where the reduced relaxation rate, T_{2r}, and reduced chemical shift, $\Delta\omega_r$, describes the iron induced change in observed transverse relaxation rate and observed chemical shift normalized to the mole fraction of coordinated water molecules (P_m). T_{2r} and $\Delta\omega_r$ receive contributions arising from the relaxation time and chemical shift of the coordinated water molecule (T_{2m}, $\Delta\omega_m$), outer sphere

contributions to relaxation and chemical shift (T_{2os}, $\Delta\omega_{os}$), and the water exchange rate, k_{ex}. The outer-sphere contribution to the observed relaxation rate is negligible and can be ignored.

For Fe^{2+}, T_{2m} is very long because of the very short electronic relaxation time of Fe^{2+} (ps) which modulates scalar relaxation, and does not contribute appreciably to the measured T_2. Fe^{2+}-PyC3A exists in the fast exchange regime over the temperature range studied ($1/T_{2r}$ is increasing with decreasing temperature). Under these conditions where $k_{ex} >> 1/T_{2m}$, $\Delta\omega_m$, T_{2r} and $\Delta\omega_r$ can be described by eqs S3-4.

$$\frac{1}{T_{2r}} = \frac{\Delta\omega_m^2}{k_{ex}} \qquad \text{(Eq S3)}$$

$$\Delta\omega_r = \Delta\omega_m \qquad \text{(Eq S4)}$$

$\Delta\omega_m$ is given by Eq S7 and increases with decreasing temperature:

$$\Delta\omega_m = \frac{2\pi g_L \mu_B S(S+1) B_o}{3k_B T} \frac{A}{h} \qquad \text{(Eq S5)}$$

where g_L is the Landé *g*-factor for a free electron, μ_B is the Bohr magneton, *S* is the spin quantum number, k_B is the Boltzmann distribution constant, B_0 is the applied magnetic field strength, and *A/h* is the Fe-^{17}O hyperfine coupling constant in MHz. *A/h* was measured by measuring the $H_2{}^{17}O$ chemical shift as a function of increasing Fe^{2+}-PyC3A concentration between 0 to 20 mM at 40 °C The temperature dependence of k_{ex} is assumed to be exponential, eq S8,

$$k_{ex} = \frac{k_{ex}^{310} T}{310.15} \exp\left[\frac{\Delta H^{\neq}}{R}\left(\frac{1}{310.15} - \frac{1}{T}\right)\right] \qquad \text{(Eq S6)}$$

where R is the universal gas constant, and $\Delta H^{\ddagger}$ is the enthalpy of activation for water exchange.

For Fe^{3+}-PyC3A, $1/T_{2r}$ is decreasing with decreasing temperature, and the system is in the slow exchange limit where $1/T_{2r}$ is the water exchange rate at each temperature, eq S9, and the chemical shift is the outer-sphere chemical shift, eq S10:

$$\frac{1}{T_{2r}} = k_{ex} \qquad \text{(Eq S7)}$$

$$\Delta\omega_r = \Delta\omega_{os} \qquad \text{(Eq S8)}$$

HPLC methods. Liquid chromatography-mass spectrometry (LC-MS) was performed using an Agilent 1100 Series HPLC interfaced to an Agilent 6130 single quadrupole electrospray mass spectrometer and to a Daly conversion dynode detector with UV detection at 220, 254, and 280 nm. The methods used on these systems are as follows: (A1) Waters X-bridge C18 column (150 × 4.6 mm , 3.5 µm particle size); eluent A: 10 mM ammonium acetate, eluent B: 95 % MeCN/10

% 10 mM ammonium acetate; gradient: 5 % B for 2 min, 5 % B to 95 % B over 8 min, 95% B for 2 min, 95% B to 5 % B for 1 min, than 5 % B for 2 min; flow rate 0.8 mL/min, (A2) Waters X-bridge C18 column (150 × 4.6 mm, 3.5 µm particle size); eluent A: 10 mM ammonium acetate, eluent B: 95 % MeCN/10 % 10 mM ammonium acetate; gradient: 5 % B for 2 min, 5 % B to 50 % B over 8 min, 95% B for 1 min, 95% B to 5 % B for 1 min, than 5 % B for 2 min; flow rate 0.8 mL/min. Reverse-phase semi-preparative purification was performed on the Rainin Dynamax HPLC system with UV detection from 220 to 280 nm using a Phenomenex C18 column (250 x 21.8 cm) The method used for purification: (P1) starting from 95% A/ 5% B held for 2 min, the fraction of B increased to 50 % over 22 min. The column was washed with 95% B for 2 min and then ramped to 5% B. The system was re-equilibrated at 5% B for 3 min.

UV-vis spectroscopy. UV-vis spectra were recorded on a SpectraMax M2 spectrophotometer using quartz cuvettes with a 1 cm path length. Extinction co-efficients (ε, $M^{-1}cm^{-1}$) were determined from the slope of a plot of absorbance for at least four concentrations of Fe complex.

Cyclic voltammetry. Cyclic voltammetry measurements were performed using a Nuvant EZstat Pro potentiostat equipped with a Ag/Ag^{+} (3 M NaCl) reference electrode, Pt wire counter electrode, and glassy carbon working electrode. Measurements were performed at room temperature using 3 mM analyte in Ar purged aqueous solutions of 0.5 M KNO_3 electrolyte. The ferri/ferrocyanide couple was used as an internal standard.[8]

Metal ion quantification. Metal concentrations were determined using an Agilent 8800-QQQ ICP-MS system. All samples with diluted with 0.1% Triton X-100 in 5% nitric acid. A linear calibration curve for metal ranging from 1.0 ppb to 1000 ppb in diluent was generated daily for the quantification.

Bulk magnetic susceptibility. The effective magnetic moments (μ_{eff}) for Fe^{3+}-PyC3A and Fe^{2+}-PyC3a were estimated using the modified Evans method based on ^{1}H NMR at 298 K.[9-11] Fe complexes were dissolved to in D_2O doped with 5% *tert*-butanol by volume and placed in a WILMAD coaxial insert tube containing blank solvent as diamagnetic reference. The molar susceptibilities were determined from the difference in *tert*-butanol chemical shift between the Fe complex solution and diamagnetic reference according to Eqs S9-10,

$$\chi_m = \chi_g \times MW \qquad \text{(Eq S9)}$$

$$\chi_g = \left|\frac{-3\Delta f}{4\pi f m} + \chi_o\right| \qquad \text{(Eq S10)}$$

where χ_g and χ_m are the mass susceptibility and molar susceptibility of the Fe complex, m is the concentration of the Fe complex in g/mL, Δf is the separation between the resonance frequencies of tert-butanol between the Fe complex solution and diamagnetic reference (in Hz), and f is Larmor frequency of water ^{1}H at the field strength of the spectrometer (499.8 MHz), and χ_O is the mass susceptibility of pure solvent (χ_o = -0.6466 x 10^{-6} mL/g for D_2O). The molar susceptibility relates directly to μ_{eff} by Eq S11, where T is temperature.

$$\mu_{eff} = 2.84\sqrt{\chi_m T} \quad \text{(Eq S11)}$$

Estimation of Fe^{3+} formation constants. Fe^{3+} formation constants were estimated from direct competition with EDTA at pH 7.4, I = 0.1 M KNO_3, RT. Product distribution at equilibrium was estimated from an HPLC analysis of the reaction mixture (HPLC method A1). The equilibrium concentrations of Fe^{3+}-PyC3A were quantified according to a linear calibration plot of HPLC peak area as a function of chelate concentration. An equilibrium constant, K_{eq}, was estimated using Eq S12,

$$K_{eq} = \frac{[PyC3A][Fe^{3+}-EDTA]}{[Fe^{3+}-PyC3A][EDTA]} \quad \text{(Eq S12)}$$

the conditional (pH 7.4) formation constant, K, was estimated from K_{eq} and the previously determined conditional K of Fe^{3+}-EDTA measured under identical conditions using Eq ~~S10~~ S13.

$$K_{eq} = \frac{K_{Fe-EDTA}}{K_{Fe-PyC3A}} \quad \text{(Eq S13)}$$

We have used this method to estimate the formation constants of Mn^{2+} complexes of PyC3A and found excellent agreement with potentiometrically determined formation constants.[12]

Estimation of Fe^{2+} formation constants. The Fe^{2+}-PyC3A formation constant were estimated by applying the Fe^{3+}-PyC3A formation constant, $Fe^{3+/2+}$-PyC3A redox potential and standard potential of the $Fe^{3+}_{(aq)}/Fe^{2+}_{(aq)}$ couple to Eq S14,[13]

$$E°_{ML} = E°_{M(aq)} - \frac{RT}{nF} ln \frac{[K_M{}^{red}{}_L]}{[K_M{}^{ox}{}_L]} \quad \text{(Eq S14)}$$

where E^o_{ML} is the redox potential of the metal complex, $E^o_{M(aq)}$ is the standard potential of the hydrated metal ion, $K_M{}^{red}{}_L$ is the formation constant of the metal complex in the reduced state, and $K_M{}^{ox}{}_L$ is the formation constant of the metal complex in the oxidized state.

Cysteine mediated reduction. The kinetics of Fe^{3+}-PyC3A reduced by cysteine were monitored spectrophotometrically via decrease of the 310 nm absorbance. All reactions were carried out at 37ºC in 100 mM pH 7.4 Tris buffer. A series of experiments where the concentrations of Fe^{3+}-

PyC3A and cysteine were varied were performed in order to estimate the rate law. Concentrations of Fe^{3+}-PyC3A were varied from 0.08 mM, 0.10 mM, 0.12 mM, and 0.14 mM, and each [Fe^{3+}-PyC3A] was reacted with 2.0 mM, 4.0 mM, and 8.0 mM of cysteine. Using a large excess of cysteine ensures that the reaction proceeds pseudo-first order with respect to Fe^{3+}-PyC3A and can be treated by Eq S15,

$$\frac{d[\mathrm{Fe^{3+}PyC3A}]}{dt} = k[\mathrm{Fe^{3+}PyC3A}] \qquad \text{(Eq S15)}$$

where the observed rate constant (k_{obs}) is the product of the actual rate constant (k) and [Cys]. In this regard, the rate law and a corresponding k were estimated by plotting reaction velocity as a function of [Fe^{3+}-PyC3A].

Glucose/ Glucose oxidase mediated oxidation. To a 0.1 mM solution of PyC3A in 100 mM Tris, pH 7.4 and 10 mM glucose, was added $FeCl_2$ solution to a final concentration of 0.1 mM Fe(II). Glucose oxidase activity was then added to initiate the H_2O_2 mediated oxidation reaction. Glucose oxidase (GOX) activity was determined by adding a 100 µL aliquot of the GOX containing mixture and a 15 U/mL horseradish peroxidase to 2 mL of an assay solution prepared from the following proportions: 26.9 mL H_2O, 3.0 mL 0.1M pH 7.0 sodium phosphate, and 0.048 mL guaiacol. Horseradish peroxidase reacts with H_2O_2 to form highly oxidizing ferryl heme species capable of guiaicol oxidation. Guaiacol oxidation was measured as a function of time via tracking the increase in absorbance at 470 nm (ε = 0.0266 $M^{-1}cm^{-1}$). 1 U GOX activity is defined as the amount of enzyme required to generate H_2O_2 at a rate of 1 µmol/min; 4 mol equiv. H_2O_2 are required to generate the 470 nm guaiacol oxidation product. We find that activity measurements are most reliable and reproducible when recorded between 1-3 min after addition of peroxidase to the assay buffer.

Transferrin competition assay, A batch of 0.1 mM Fe^{3+}-PyC3A was incubated with 0.1 mM apotransferrin in pH 7.0 buffer containing 50 mM HEPES and 25 mM $NaHCO_3$. The reaction was monitored by spectrophotometrically at 465 nm for release of Fe^{3+} from Fe^{3+}-PyC3A to transferrin (ε = 4950 M^{-1} cm^{-1}) over the course of 24 h.

Mouse model of acute pancreatitis. We used the caeurlean/LPS model of severe acute pancreatitis.[14] Briefly, male balb/C mice were treated with six hourly intraperitoneal (i.p.) doses of 50 µg/ kg caerulein initiated 18 h before imaging, 3 h before imaging mice were treated with an i.p. dose of 10 mg/kg lipopolysaccharide (LPS). Vehicle treated control mice were treated with an identical regimen of saline injections. After imaging, mice were euthanized by cardiac puncture

and the pancreas was removed and processed for spectrophotometric MPO assay and histopathology.

Magnetic Resonance Imaging. Magnetic resonance imaging was performed using a Bruker Biospec 4.7T system.

Phantoms. Samples were placed in a homemade sample holder and imaged using a volume coil. The sample holder accommodates simultaneous measurement of up to 5 samples of varying concentration. T_1 values for each compound was determined using a 2D rapid acquisition refocused echo (RARE) inversion recovery sequence. Echo time = 7.0 ms, repetition time ranging from 50-5000 ms for Fe^{2+}-PyC3A and 50-3000 ms for Fe^{2+}-PyC3A, acquisition matrix = 90 x 48, field of view = 45 x 24 mm, slice thickness 2 mm. T_1 measurements were performed on Fe^{3+}-PyC3A samples ranging between 0.2 - 1.0 mM and Fe^{3+}-PyC3A samples ranging between 2.0 - 8.2 mM. T_1 was obtained from a nonlinear least square fit of the signal intensity (SI(t)) vs TI curve where T_1, SI(0) and *a* are adjustable parameters, equation S16,

$$\mathrm{SI(t)} = \mathrm{SI(0)}[1 - \mathrm{a} \times \mathrm{e}^{\mathrm{TI/T1}}] \qquad \text{(Eq S16)}$$

where $M_z(0)$ is the equilibrium magnetization, *TI* is the inversion time, and *TR* is the repetition time.

T_1-weighted images were obtained using a 2D fast low angle shot (FLASH) gradient echo sequence: repetition time/ echo time/ flip angle = 125 ms/ 2.96 ms/ 60°; acquisition matrix = 220 x 220, field of view = 33 x 33 mm, slice thickness 2 mm, acquisition time = 1 min, 50 s.

Dynamic MR imaging. Mice were imaged with a 3D T_1-weighted FLASH sequence (coronal orientation) at baseline and every 1 minute out to 6 min following tail vein injection of 0.2 mmol/kg of Fe^{3+}-PyC3A or Fe^{2+}-PyC3A (formulated as 50 mM aqueous solution). *Imaging parameters*: TR/TE/flip angle=15 ms/2.46 ms/25°, in-plane FOV = 47.365 x 28.026 mm, matrix=120×70, 50 slices, slice thickness = 0.4 mm, voxel size = 0.4 x 0.4 x 0.4 mm, 1 average, and acquisition time = 0 min, 52 s).

Pancreatitis imaging. Mice were imaged with a series of alternating axial and coronal 2D T_1-weighted FLASH sequences prior to and out to 33 min following tail vein injection of 0.2 mmol/kg Fe^{2+}-PyC3A or 0.02 mmol/kg Mn^{2+}-PyC3A. TR/TE/flip angle=135 ms/2.93 ms/60°, in-plane FOV = 33x33 mm, matrix = 140×140, 9 slices, slice thickness = 1.0 mm, 8 averages, and acquisition time = 2 min, 31s.

Contrast-to-noise ratios (CNR) were quantified from the axial 2D images. Axial slices consistently provided substantial cross sections of pancreas and psoas muscle for quantitation of pancreas vs. muscle CNR.

Immunohistochemical myeloperoxidase staining. OCT-embedded pancreatic tissues were sectioned, and slides were kept in -80 prior to staining. For immunohistochemical detection of myeloperoxidase, slides were air dried for 5 minutes in room temperature (RT) and then fixed in cold acetone for 20 minutes in -20°C following washing in PBS. After blocking of endogenous peroxidase using 3% hydrogen peroxide (Fisher Scientific, USA) for 2 hours in RT and incubation with Power Block Universal Blocking Reagent (1X) (BioGenex Laboratories, USA) for 1 hour in RT, sections were permeabilized with 2% Triton-X100 for 20 minutes at RT. Next, a polyclonal mouse anti-MPO antibody (DAKO, USA) or a polyclonal rabbit anti-CD11b (Novus Biologicals, USA) was applied in a dilution of 1:200 in Antibody diluent solution (Sigma Millipore, USA) for overnight in 4 °C. After 10 minutes wash with PBST, sections were incubated with biotinylated anti-mouse or anti rabbit IgG (Sigma Millipore, USA) for 30 minutes at RT and subsequently with streptavidin-horseradish peroxidase conjugate (Sigma Millipore, USA) for 10 minutes at RT. After 10 minutes wash with phosphate buffered saline with Tween (PBST), Metal-Enhanced DAB Substrate (Thermo Fisher Scientific, USA) was applied for 2 minutes to visualize the immunostaining. Counterstaining was performed using Mayer's Hematoxylin (Sigma-Aldrich, USA).

Peroxidase activity quantification. Pancreatic tissue was homogenized with a tissue homogenizer in 20 mM sodium phosphate, pH 7.4, then centrifuged for 10 minutes at 13,000 x g. The supernatant was discarded and the pellet re-suspended by pipetting in 50 mM sodium phosphate with 0.5% w/v hexadecylmethylammonium bromide, pH 6.0. This suspension was subjected to four freeze-thaw cycles, then samples placed in an ice slurry and sonicated with a bath sonicator for three minutes. The suspensions were centrifuged for 10 minutes at 13,000 x g the supernatant was assayed for peroxidase activity as previously described.[15-16]. Briefly, a 100 µL aliquot of pancreatic tissue digest was added to 2 mL of an assay solution prepared from the following proportions: 26.9 mL H_2O, 3.0 mL 0.1M pH 7.0 sodium phosphate, 0.1 mL of 0.1M H_2O_2, and 0.048 mL guaiacol. Guaiacol oxidation was measured as a function of time via tracking the increase in absorbance at 470 nm ($\varepsilon = 0.0266\ M^{-1}cm^{-1}$). 1 U peroxidase is defined as the amount of enzyme required to react with H_2O_2 at a rate of 1 µmol/min; 4 mol equiv. H_2O_2 is required to

generate the 470 nm guaiacol oxidation product. We find that activity measurements are most reliable and reproducible when recorded between 1-3 min after addition of peroxidase to the assay buffer.

Synthesis. The ligand PyC3A was synthesized as previously described.[12]

Fe^{3+}-PyC3A. $FeCl_3$ (0.041 g, 252 μmol) was added to a 4 ml water solution of ligand (0.100 g, 264 μmol). pH was adjusted to neutral by adding 1 M NaOH. Complex formation was monitored by LC-MS. The reaction mixture was subject to preparative HPLC (method P1) purification. The product was isolated as a pale yellow solid (0.064, 148 μmol, 56%) in 98% purity as determined by HPLC (method A1). UV-vis (H_2O, 25 °C) λ_{max}, ε (nm, $M^{-1}cm^{-1}$): 250 (10,810), 310, (5,440). ESI-MS: m/z = 433.1, $[M+H]^+$; calcd.: 433.1.

Fe^{2+}-PyC3A. In situ complexation*:* To a solution of 0.5 mM of PyC3A in 100 mM PIPES buffer was added 0.95 equiv. of 100 mM $FeCl_2$ solution. The solution was gently mixed in a sealed vial.. In situ reduction by sodium ascorbate*:* To a solution of 0.5 mM of Fe^{3+}-PyC3A in 100 mM PIPES was added 10 equiv. of 100 mM sodium ascorbate. The solution was gently mixed until bright yellow color formed. 5 min after mixing, An aliquot was removed for LC-MS characterization to ensure the reduction was complete. Formulation for intravenous injection: To a solution of 50 mM Fe^{3+}-PyC3A in water was added 0.5 equiv. 1M sodium ascorbate, the solution was gently shaken by hand until bright yellow color was observed. The required volume of this solution was drawn for intravenous injection. Fe^{2+}-PyC3A solutions were prepared on site no more than 30 min prior to intravenous injection. UV-vis (H2O, 25 °C) λ_{max}, ε (nm, $M^{-1}cm^{-1}$): 215 (4,610), 300 (2,020), 400 (670), 475 (100). ESI-MS: m/z = 434.1, $[M+H]^+$; calcd.: 434.1.

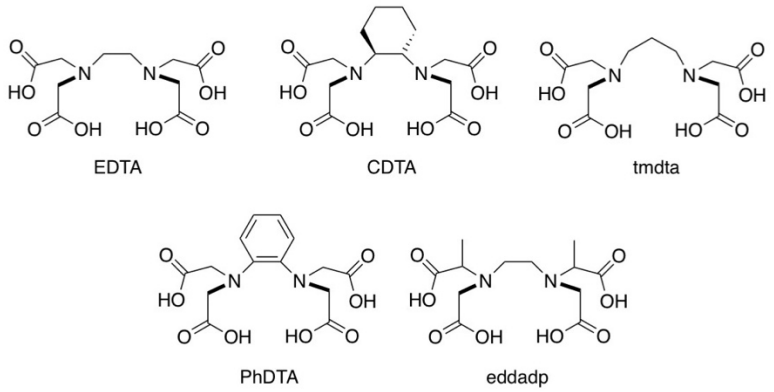

Figure S1. Ligands used for Fe complexes discussed in the manuscript.

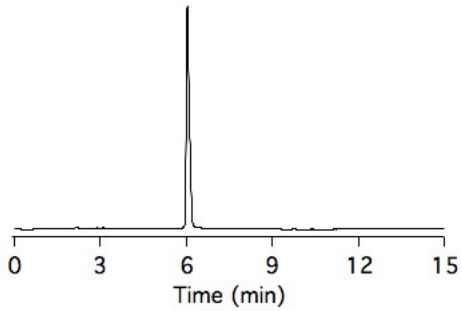

Figure S2. HPLC trace (method A1) of Fe^{3+}-PyC3A at 254 nm detection.

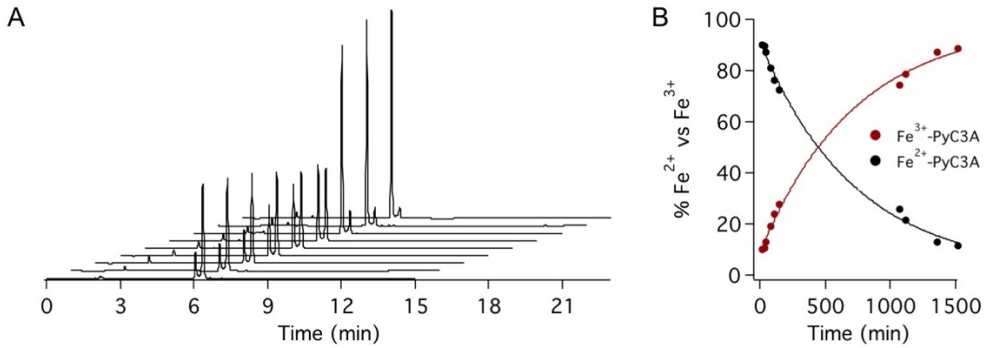

Figure S3. (A) Aerobic oxidation of 0.5 mM Fe^{2+}-PyC3A generated in situ (PyC3A + $FeCl_2$ in pH 7.0 PIPES) monitored by HPLC as a function of time after initial chelate formation. The peaks at t_R = 6.4 min and 6.1 min correspond to Fe^{2+}-PyC3A and Fe^{3+}-PyC3A, respectively. The traces were recorded at (front to back) 17, 25, 49, 82, 114, 146, 1076, and 1119 min after formation of the Fe^{2+} complex. (B) Plot of Fe^{2+}- vs Fe^{2+}-PyC3A speciation as a function of time. Under these conditions, oxidation occurs with a $t_{1/2}$ of 8.4 h.

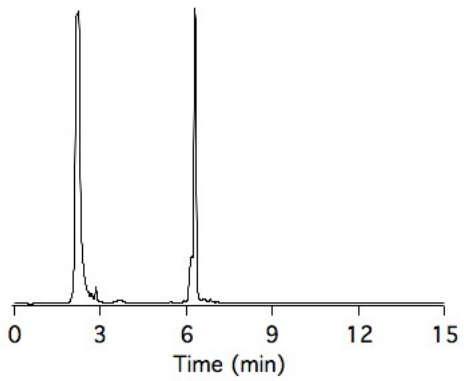

Figure S4. HPLC trace (method A1) of Fe^{2+}-PyC3A (t_R = 6.4 min) generated in situ by reduction of Fe^{3+}-PyC3A with 10 mol. equiv. ascorbate (t_R = 2.4 min).

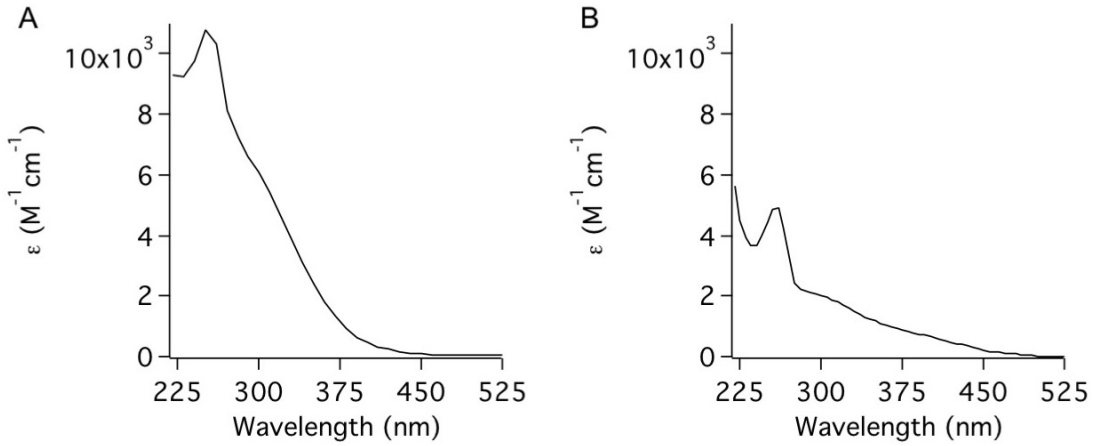

Figure S5. UV-vis traces of Fe^{3+}-PyC3A (A) and Fe^{2+}-PyC3A (B) in water.

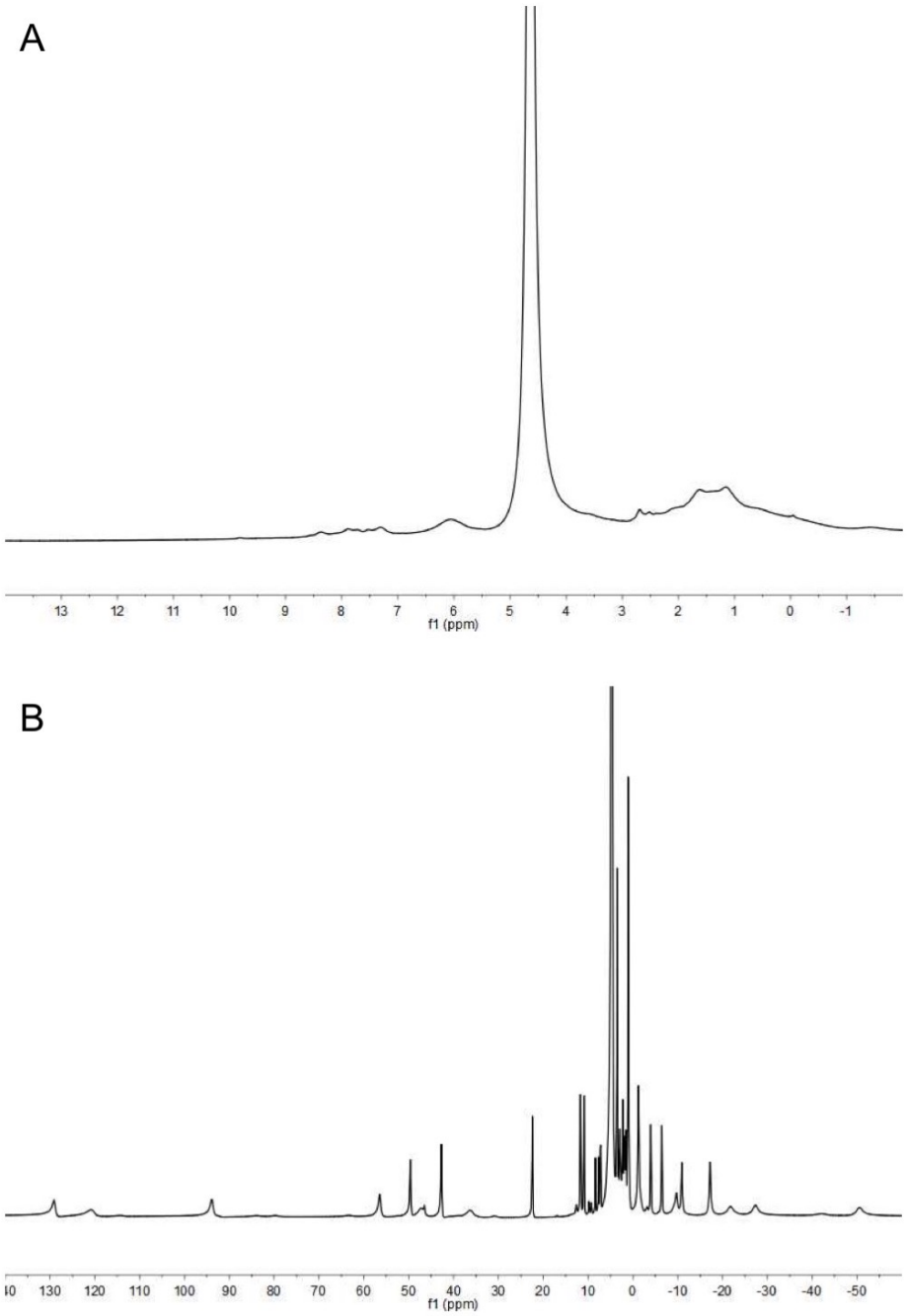

Figure S6. ^{1}H NMR spectra of (A) Fe^{3+}-PyC3A and (B) Fe^{2+}-PyC3A in D_2O recorded at 11.7T. (A) The ^{1}H resonances of Fe^{3+}-PyC3A are broadening into the baseline and indiscernable, consistent with the presence of high-spin Fe^{3+}. (B) The ^{1}H resonances of Fe^{2+}-PyC3A are dispersed between -60 and 140 ppm. Based on prior reports of the ^{1}H NMR spectra of Fe^{2+}-CDTA,[4] the sharp resonances locates between 50 and -20 ppm are tentatively attributed to the rigid *trans*-cyclohexylene-1,2-diamine backbone, and the broadened resonances are attributed to ^{1}H located on the carboxylate and pyridyl donor arms. More than 22 unique chemical shifts are observed, which we attribute to a mixture of Δ and Λ isomers.[4]

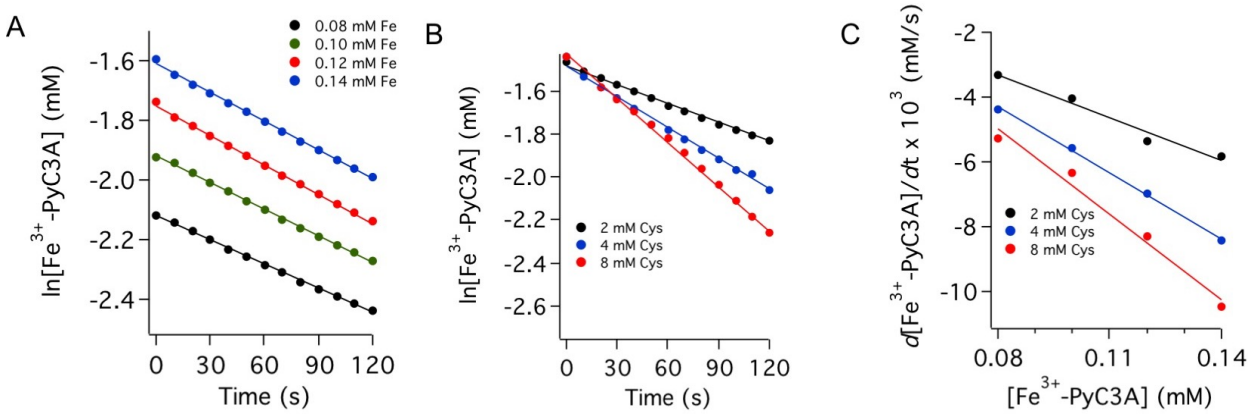

Figure S7. (A-C) The kinetics of Fe^{3+}-PyC3A reduction by cysteine were measured under pseudo-first order conditions with respect to Fe^{3+}-PyC3A. (A) Reduction of different concentrations of Fe^{3+}-PyC3A ranging between in the presence of 2 mM cysteine. (B) Reduction of 0.14 mM Fe^{3+}-PyC3A in the presence of varying concentrations of cysteine ranging between 2-8 mM. (C) Plots of initial rates of reduction of 0.08, 0.10, 0.12 and 0.14 mM solutions of Fe^{3+}-PyC3A as a function of varying cysteine concentration. The reaction is first order with respect to both [Fe^{3+}-PyC3A] and [cysteine], with $k = 1.5 \pm 0.3$ $M^{-1}s^{-1}$.

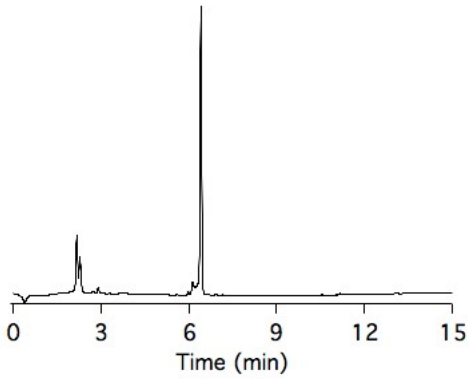

Figure S8. HPLC trace (method A1) of Fe^{2+}-PyC3A (t_R = 6.4 min) generated in situ by reduction of Fe^{3+}-PyC3A with 10 mol. equiv. L-cysteine (t_R = 2.2 min).

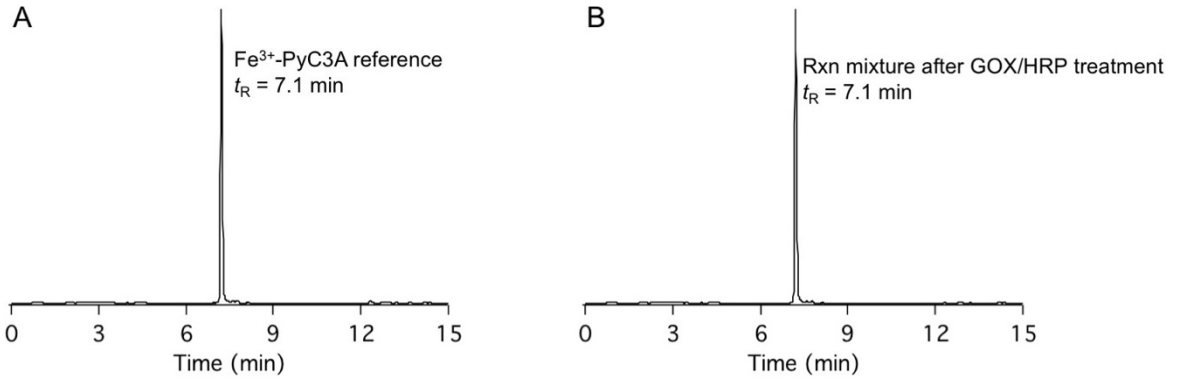

Figure S9. HPLC traces recorded on solutions after incubating 0.5 mM Fe^{2+}-PyC3A with 0.10 U glucose oxidase (A) and 15 U/ml horseradish peroxidase (B) indicate clean oxidation to Fe^{3+}-PyC3A (t_R = 7.1 min, HPLC method A2) without formation of degradation byproducts.

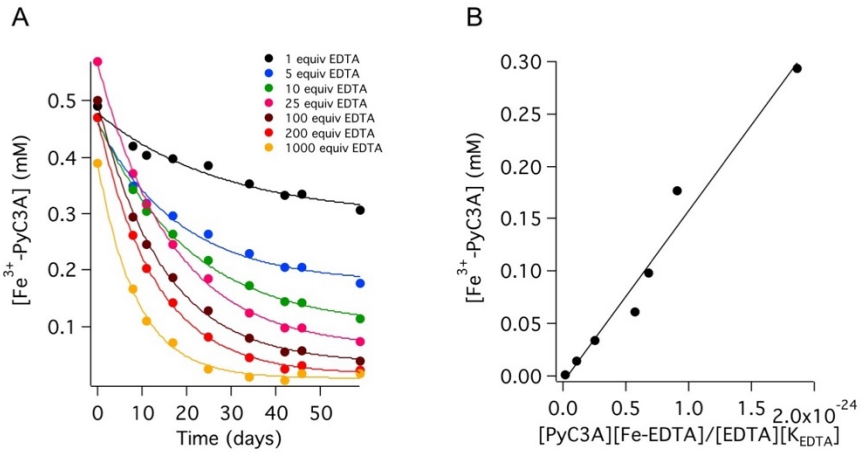

Figure S10. (A) The competition reactions between 0.5 mM Fe^{3+}-PyC3A and varying concentrations of EDTA at pH 7.4 (I = 0.15 M KCl) were monitored over the course of 59 days. (B) The conditional pH 7.4 equilibrium constant ($K_{pH\ 7.4}$) for Fe^{3+}-PyC3A was determined from the slope of a plot of Fe^{3+}-PyC3A concentration at equilibrium against [PyC3A][Fe-EDTA]/[EDTA][$K_{Fe\text{-}EDTA}$].

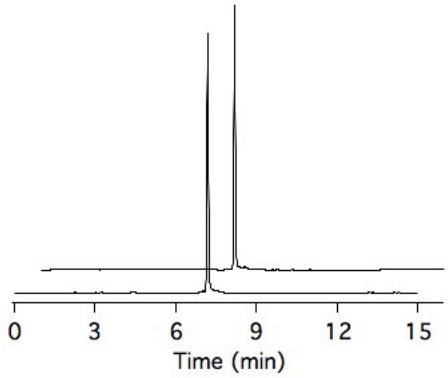

Figure S11. Comparison of HPLC traces of 1.0 mM Fe^{3+}-PyC3A prior to (foreground) and 72 h after challenge with 20 mM $Zn^{2+}(OTf)_2$ (offset) indicate <0.4% of Fe^{3+} is displaced by Zn^{2+}.

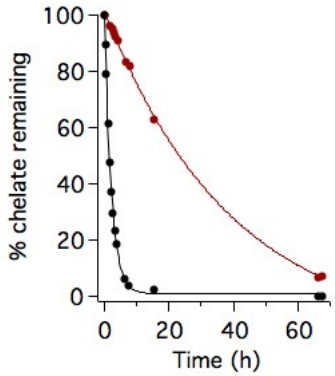

Figure S12. Fe^{2+}-PyC3A (red trace) and Mn^{2+}-PyC3A (black trace) (1.0 mM each) were challenged with 20 mM $Zn^{2+}(OTf)_2$ at pH 6.0 and the trans-chelation reactions monitored by HPLC. Fe^{2+}-PyC3A is 18 times more kinetically inert than the corresponding Mn^{2+} complex, which has been shown to be very robust to degradation and excreted intact in vivo.

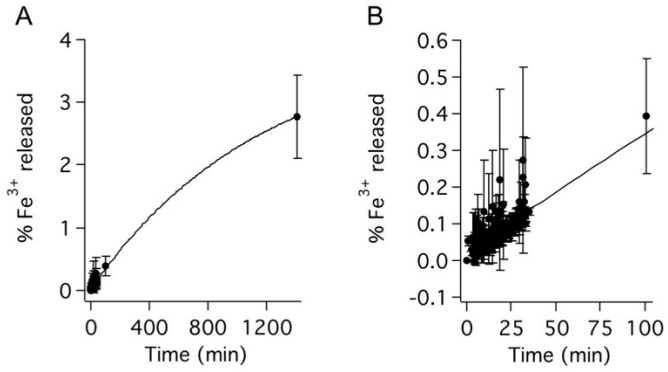

Figure S13. (A) Transfer of Fe^{3+} from PyC3A to transferrin was monitored spectrophotometrically at 465 nm over the course of 24 h (1440 min). (B) Data points collected between 0 and 110 min of transferrin incubation experiment. Note the compressed y-axis scale. Conditions: 0.1 mM Apo-transferrin, 0.1 mM Fe^{3+}-PyC3A, 25 mM $NaHCO_3$, 50 mM HEPES, pH 7.4, RT.

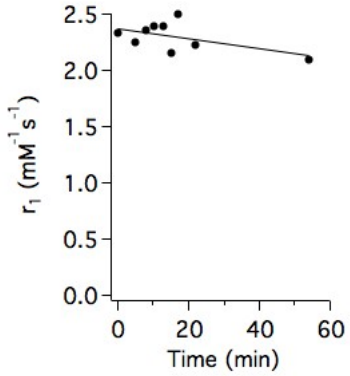

Figure S14. Mn^{2+}-PyC3A is a redox inert, negative control for Fe^{2+}-PyC3A. The complex does not undergo significant r_1 change (1.4T, 37 °C) upon incubation with glucose oxidase/ horseradish peroxidase (0.1 U/mL).

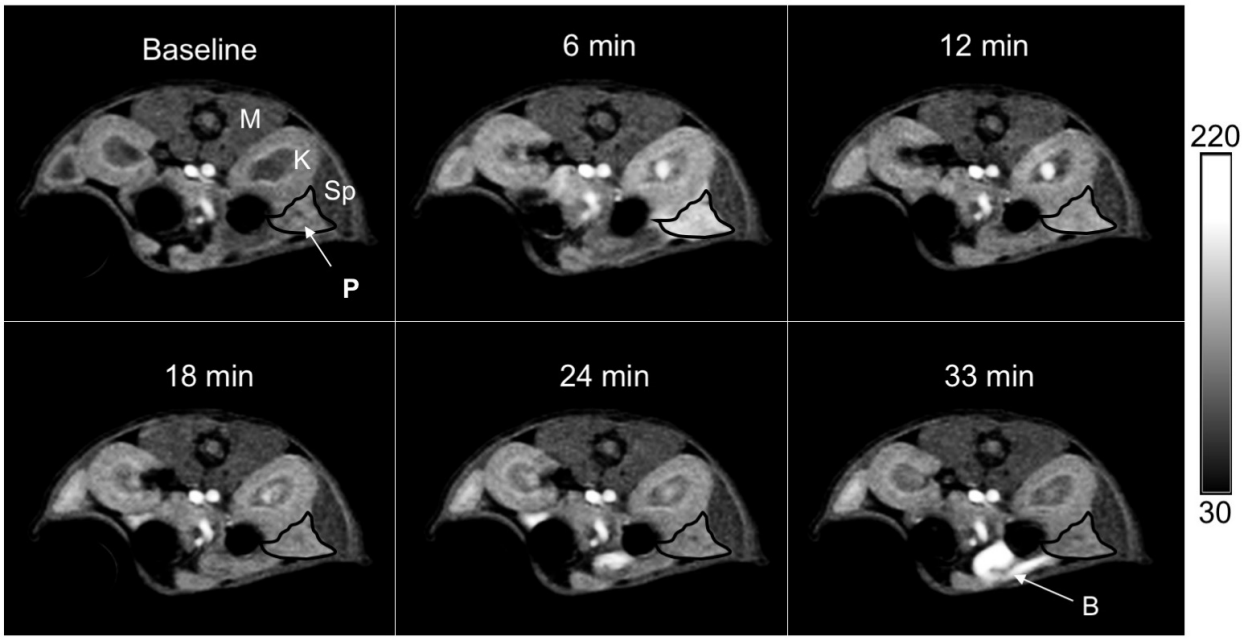

Figure S15. T1-weighted axial images recorded prior to and out to 33 min after injection of Fe2+-PyC3A to caerulein/ LPS treated mouse. The pancreas (denoted by P) is strongly and selectively enhanced during the early (6 and 12 min) time points but signal rapidly diminishes to baseline consistent with rapid washout of the low molecular weight agent. Strong enhancement is observed in the kidney pelvis during the early time points due to accumulation of high concentrations of contrast agent, but diminishes as Fe-PyC3A passes into the urine. During the delayed time points (24 min, 33 min) enhancement of the bowel (denoted by B) is observed, presumably due to partial hepatobiliary clearance of the agent.

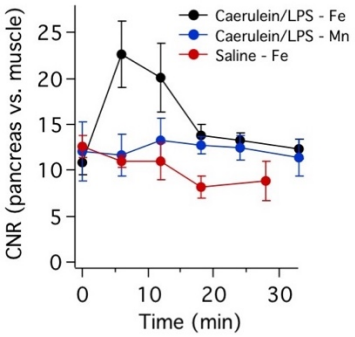

Figure S16. Time course of pancreas vs. muscle contrast-to-noise ratio (CNR) following injection of Fe^{2+}-PyC3A to caerulein/ LPS and saline treated mice, and after injection of Mn^{2+}-PyC3A to caerulein/ LPS treated mice.

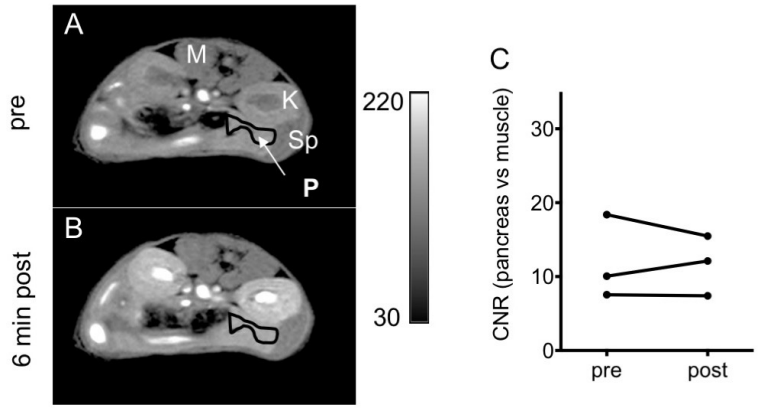

Figure S17. T_1-weighted 2D axial images of caerulein/LPS treated mice recorded (A) prior to and (B) 6 min after injection of Mn^{2+}-PyC3A. Organs are labelled as follows: P = pancreas, Sp = spleen, K = kidney, M = muscle. The change in pancreas vs. muscle CNR measured pre contrast agent injection compared to post contrast agent injection is not significant, CNR_{pre} = 12±5.7, CNR_{post} = 12±4.1, post-pre ΔCNR = -0.33±2.5, N = 3, P = 0.84, two-sided t-test (C).

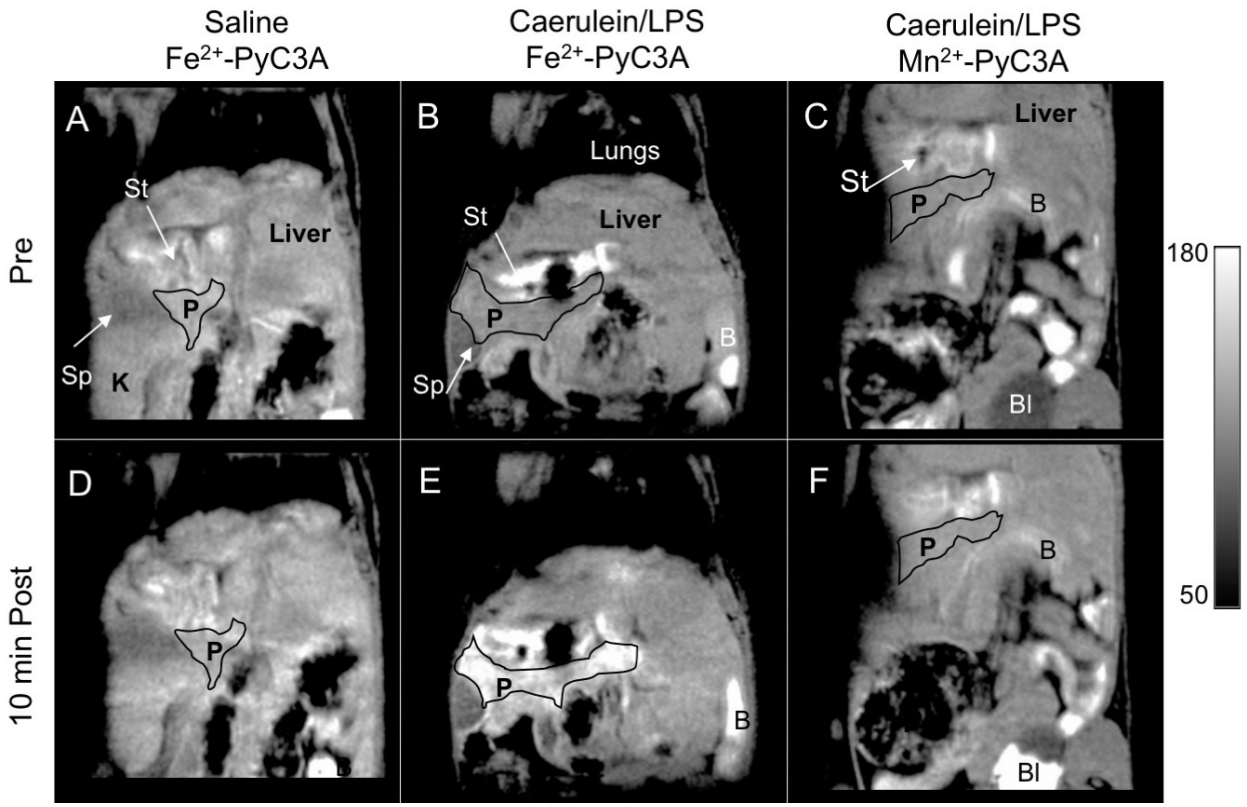

Figure S18. T_1-weighted 2D coronal images of saline and caerulein/LPS treated mice recorded prior to and 10 min after injection of Fe^{2+}-PyC3A or Mn^{2+}-PyC3A. Organs are labelled as follows: P = pancreas, L = Liver, Sp =spleen, St = stomach, K = kidney, M = muscle, B = bowel. Bl = Bladder. Note that pancreas, and liver are isointense prior to contrast injection (A-C), after injection of Fe^{2+}-PyC3A to saline treated mice (D), or after injection of Mn^{2+}-PyC3A to caerulein/ LPS treated mice (F), but that the pancreas is strongly and selectively enhanced after injection of Fe^{2+}-PyC3A to caerulein/ LPS treated mice (E). The bowel and stomach are strongly enhanced at all times because of high levels of metals including Mn present in the mouse chow.

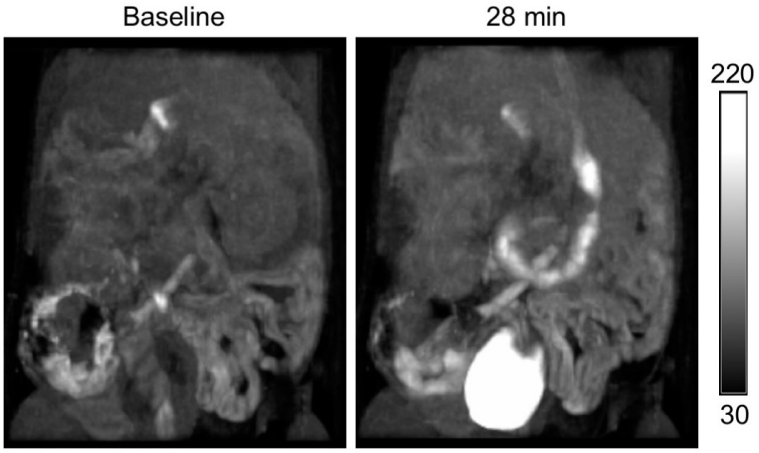

Figure S19. Maximum intensity projections of T_1-weighted coronal images recorded prior to and 28 min after injection of Fe^{2+}-PyC3A to caerulein/ LPS treated mouse. The strong contrast enhancement in the bladder and bowel at the delayed time point is consistent with excretion of the Fe-PyC3A. The is no excretory mechanism for de-chelated Fe.

	q	***A/h* (MHz)**	k_{ex}^{310} **x** 10^{-6} **(s^{-1})**	τ_m^{310} **(ns)**	$\Delta H^{\ddagger}$ **(kJ/mol)**
Fe^{3+}-PyC3A	1	N/D	2.5 ± 0.1	394 ± 6	23.2 ± 0.9
Fe^{3+}-EDTA[5]	1	65	109	9.14	24.3
Fe^{3+}-CDTA[7]	1	66	21.0	47.5	27.0
Fe^{3+}-eddadp[7]	1	N/D	148	6.75	26.0
Fe^{3+}-PhDTA[7]	1	N/D	19.2	81.4	26.0
Fe^{3+}-tmdta[4]	1	N/D	28.1	35.5	43.0
Fe^{2+}-PyC3A	1	6.8	277 ± 5	3.6 ± 0.1	5.9 ±0.5
$Fe^{2+}(H2O)_6$[17]	6	9.4	8.7	115	41.4
Fe^{2+}-EDTA[6]	1	10	6.64	150	43.0
Fe^{2+}-CDTA[4]	1	10	298	3.36	15.7
Fe^{2+}-tmdta[4]	1	10	223	4.48	42.0

Table S1. Comparison of number of water co-ligands (*q*), and corresponding water exchange parameters recorded for Fe^{3+}- and Fe^{2+}-PyC3A and previously reported complexes of high-spin Fe^{3+} and high-spin Fe^{2+}. *A/h* = Fe-^{17}O hyperfine coupling constant, k_{ex}^{310} = rate of water co-ligand exchange at 37 °C, τ_m^{310} = mean residency time of water co-ligand at 37 °C.

References

1. Fulmer, G. R.; Miller, A. J. M.; Sherden, N. H.; Gottlieb, H. E.; Nudelman, A.; Stoltz, B. M.; Bercaw, J. E.; Goldberg, K. I., NMR chemical shifts of trace impurities: common laboratory solvents, organics, and gases in deuterated solvents relevant to the organometallic chemist. *Organometallics* **2010,** *29* (9), 2176-2179.
2. Swift, T. J.; Connick, R. E., NMR-Relaxation Mechanisms of O17 in Aqueous Solutions of Paramagnetic Cations and the LIfetime of Water Molecules in the First Coordination Sphere. *J. Chem. Phys.* **1962,** *37* (2), 307-320.
3. Brausam, A.; Maigut, J.; Meier, R.; Szilagyi, P. A.; Buschmann, H.-J.; Massa, W.; Homannay, Z.; van Eldik, R., Detailed Spectroscopic, Thermodynamic, and Kinetic Studies on the Protolytic Equilibria of FeIIIcydta and the Activation of Hydrogen Peroxide. *Inorg. Chem.* **2009,** *48* (16), 7864-7884.
4. Maigut, J.; Meier, R.; Zahl, A.; van Eldik, R., Effect of chelate dynamics on water exchange reactions of paramagnetic aminopolycarboxylate complexes. *Inorg. Chem.* **2008,** *47* (13), 5702-5719.
5. Maigut, J.; Meier, R.; Zahl, A.; van Eldik, R., Triggering Water Exchange Mechanisms via Chelate Architecture. Shielding of Transition Metal Centers by Aminopolycarboxylate Spectator Ligands. *J. Am. Chem. Soc.* **2008,** *130*, 14556-14569.
6. Maigut, J.; Meier, R.; Zahl, A.; van Eldik, R., Elucidation of the Solution Structure and Water-Exchange Mechanism of Paramagnetic [FeII(edta)(H2O)]2-. *Inorg. Chem.* **2007,** *46* (13), 5361-5371.
7. Schneppensieper, T.; Seibig, S.; Zahl, A.; Tregloan, P.; van Eldik, R., Influence of Chelate Effects on the Water-Exchange Mechanism of Polyaminecarboxylate Complexes of Iron(III). *Inorg. Chem.* **2001,** *40* (15), 3670-3676.
8. O'Reilly, J. E., OXIDATION-REDUCTION POTENTIAL OF FERRO-FERRICYANIDE SYSTEM IN BUFFER SOLUTIONS. *Biochim. Biophys. Acta* **1973,** *292* (3), 509-515.
9. Evans, D. F., 400. The determination of the paramagnetic susceptibility of substances in solution by nuclear magnetic resonance. *J. Chem. Soc.* **1959**, 2003-2005.
10. Löliger, J.; Scheffold, R., Paramagnetic Moment Measurements by NMR. A Micro Technique. *J. Chem. Ed.* **1972,** *49*, 646-647.
11. Shin, B.; Sutherlin, K. D.; Ohta, T.; Ogura, T.; Solomon, E. I.; Cho, J., Reactivity of a Cobalt(III)–Hydroperoxo Complex in Electrophilic Reactions. *Inorg. Chem.* **2016,** *55*, 12391-12399.
12. Gale, E. M.; Atanasova, I.; Blasi, F.; Ay, I.; Caravan, P., A Manganese Alternative to Gadolinium for MRI Contrast. *J. Am. Chem. Soc.* **2015,** *137* (49), 15548-15557.
13. Rorabacher, D. B., Electron Transfer by Copper Centers. *Chem. Rev.* **2004,** *104*, 651-697.
14. Ding, S.-P.; J.-C., L.; Jin, C., A mouse model of severe acute pancreatitis induced with caerulein and lipopolysaccharide. *World J. Gastroenterol.* **2003,** *9* (3), 584-589.
15. Klebanoff, S. J.; Waltersdorph, A. M.; Rosen, H., Antimicrobial Activity of Myeloperoxidase. *Methods in Enzymology* **1984,** *105* (52), 399-403.
16. Nahrendorf, M.; Sosnovik, D.; Chen, J. W.; Panizzi, P.; Figueiredo, J.-L.; Aikawa, E.; Libby, P.; Swirski, F. K.; Weissleder, R., Activatable Magnetic Resonance Imaging Agent Reports Myeloperoxidase Activity in Healing Infarcts and Noninvasively Detects the Antiinflammatory Effects of Atorvastatin on Ischemia-Reperfusion Injury. *Circulation* **2008,** *117*, 1153-1169.

17. Ducommun, Y.; Newman, K. E.; Merbach, A. E., High-pressure 1 7 0 NMR Evidence for a Gradual Mechanistic Changeover from I, to Id for Water Exchange on Divalent Octahedral Metal Ions Going from Manganese(II) to Nickel(II). *Inorg. Chem.* **1980,** *19*, 3696-3703.